Resonance Raman measurements of carotenoids using light-emitting diodes

Scott D. Bergeson
Justin B. Peatross
Brigham Young University
Department of Physics Astronomy
Provo, Utah 84602

N. Jay Eyring
John F. Fralick
Douglas N. Stevenson
Scott B. Ferguson
Pharmanex Research Institute
75 West Center
Provo, Utah 84601

Abstract. We report on the development of a compact commercial instrument for measuring carotenoids in skin tissue. The instrument uses two light-emitting diodes (LEDs) for dual-wavelength excitation and four photomultiplier tubes for multichannel detection. Bandpass filters are used to select the excitation detection wavelengths. The $f/1.3$ optical system has high optical throughput and single photon sensitivity, both of which are crucial in LED-based Raman measurements. We employ a signal processing technique that compensates for detector drift and error. The sensitivity and reproducibility of the LED Raman instrument compares favorably to laser-based Raman spectrometers. This compact, portable instrument is used for noninvasive measurement of carotenoid molecules in human skin with a repeatability better than 10%. © *2008 Society of Photo-Optical Instrumentation Engineers.*
[DOI: 10.1117/1.2952075]

1 Introduction

Carotenoids are important in maintaining proper human health. They protect tissues from oxidative stress that might otherwise lead to premature macular degeneration,[1] cataract formation,[2] premature skin aging, and basal cell and squamous cell carcinomas.[3,4] Carotenoids protect cellular DNA[5] and play a role in the recovery of burn patients.[6] Reliable monitoring of carotenoid levels in tissue may aid studies to better understand how they perform these functions.

Resonance Raman spectroscopy has been demonstrated as a rapid, noninvasive approach to monitoring carotenoid concentrations in human tissues.[7,8] The method's success is primarily due to the low fluorescence quantum yield of these molecules. While the Raman scattering cross section increases dramatically on resonance, fluorescence from carotenoids remains low.

Several compact laser-based Raman spectrometers have been reported.[4,7–12] Typically these use optical fibers to deliver laser light to the sample and to collect scattered light. Grating spectrometers and charge-coupled device (CCD) detectors are used to disperse and detect the scattered light spectrum. This approach offers wide spectral coverage, aiding in the identification of several biomolecules in the sample. Fiber coupling of the laser and fluorescence collection is convenient because the mode diameter and numerical aperture of the fiber is a good match for both the laser and spectrometer. These systems often require environmentally stable operating conditions. The performance of the lasers and CCD detectors are sensitive to temperature variations. In an unstable environment, frequent recalibrations are required.

The large resonance Raman scattering cross section makes it possible to use incoherent excitation sources, such as light-emitting diodes (LEDs). These sources can offer higher stability in a wider range of environmental conditions at a lower cost and in a small form factor. However, these sources have broad spectral bandwidths, do not couple well into optical fibers, and are poorly matched to the slit area and numerical aperture of grating spectrometers. Using a bandwidth-narrowed LED source with a conventional Raman spectrometer results in recorded spectra that are one to two orders of magnitude weaker than those measured using a laser source.

This lower signal level can be overcome in part with sensitive detectors. For example, an instrument for measuring carotenoids in the macula was reported.[13] A photomultiplier tube (PMT) was used to detect the Raman signal transmitted through a narrowband interference filter. By tilting the filter, it was possible to change the passband wavelength enough to determine the baseline fluorescence level at a nearby wavelength and to subtract this from the Raman signal. Because the signal-to-background levels were relatively high (0.20), changes in the background fluorescence only had a small influence on these carotenoid measurements.

We describe an instrument that uses spectrally filtered LEDs for resonance Raman spectroscopy of carotenoids in skin tissue. For a narrowband excitation source, the signal-to-background ratio is 20 times smaller in the skin than in the macula, 1% being a typical value. For a spectrally filtered LED, this ratio is even smaller, owing to the 1-nm spectral width of the bandwidth narrowing filter. Such an excitation source emits only 0.5 mW of optical power, resulting in an order of magnitude less of light exposure to the skin tissue,

Address all correspondence to: Scott D. Bergeson, Department of Physics and Astronomy, Bringham Young University, N283 ESC, Provo, Utah 84602. Tel: 801 422 6161; Fax: 801 422 0553; E-mail: scott.bergeson@byu.edu

and therefore much lower signal levels compared with a typical laser-based instrument.

We also describe techniques we developed to overcome the difficulties in using low-intensity excitation sources. We use PMTs to measure the skin fluorescence for increased sensitivity. To compensate for both short- and long-term drifts in detector sensitivity inherent to PMTs, we exploit a dual-wavelength excitation method. These detectors are not stable enough to use traditional shifted excitation Raman difference spectroscopy (SERDS).[14] Because the signal-to-background ratio is so small, minor variation in the detector gain on the one-minute time scale can compromise measurements of the Raman signal. Rather than subtract, we divide the spectra from the two excitation sources. This cancels detector gain variation on a one-second time scale. In this regime, it is also essential to control for spatial and optical polarization differences from the two excitation sources. If not controlled, either of these can introduce errors comparable to or larger than the Raman line. These techniques are incorporated into a compact commercial instrument with good measurement repeatability under widely varying ambient conditions. We demonstrate calibration stability over a period of nine months, and it seems likely that much longer stability times can be maintained.

2 Carotenoid Spectroscopy

The optical properties of carotenoids have been studied extensively over the past few decades. A variety of fluorescence, excited-state absorption, and Raman methods have clarified carotenoid energetics and given insight into how these molecules perform their various chemical roles.[15–18] In skin tissue, lycopene and β-carotene are the dominant carotenoid molecules.[8] They both have a backbone of nine conjugated carbon bonds, with additional conjugation into ionone rings on each end.

Optical excitation of carotenoids occurs in the blue-green spectral region, between 400 and 500 nm. The three Raman lines in β-carotene are at 1008 cm^{-1} ($C—CH_3$ rocking mode), 1159 cm^{-1} ($C—C$ stretch mode), and 1525 cm^{-1} ($C{=}C$ stretch mode), with the latter being the strongest. Because of fast nonradiative relaxation, spontaneous fluorescence is suppressed, with a fluorescence quantum yield of only 10^{-5}.[7,17] The fluorescence background is dominated by contributions from other tissue components (lipids, proteins, melanin, DNA, hemoglobin, etc.[19]). The resulting Raman signal-to-background ratio is typically 1%.[20,21]

3 Optical Design

Our application focuses on detection of the 1525 cm^{-1} Raman line in human skin tissue under resonance excitation conditions. The optical layout is shown in Fig. 1. A blue LED is used as the excitation source. Its nominal 25-nm [full width at half maximum (FWHM)] spectral width is narrowed to 0.8 nm using a bandpass filter at 473 nm. This light reflects from a dichroic mirror and is focused onto the sample. Fluorescence and the Raman signal from the sample passes back through the dichroic mirror. A series of partially reflecting beamsplitters divides the optical signal into four channels. Light in each channel passes through an additional 1-nm bandpass filter and is detected using a photomultiplier tube (PMT). The four 1-nm detection bandpass filters have centers
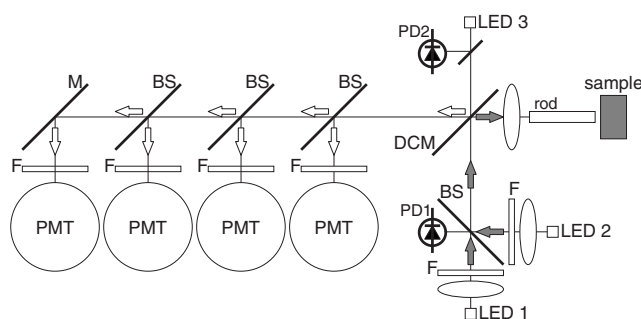

Fig. 1 Schematic diagram of the optical layout of our instrument. M =mirror, BS=beamsplitter, DCM=dichroic mirror, F=bandpass filter, L=lens, and PD=photodiode. Bandpass filter properties are noted in the text. The optical power at the sample is less than 0.5 mW in 3.1 mm^2.

spaced equally on 2-nm intervals. The center wavelengths of the detection filters are chosen so that one of the filters is shifted 1525 cm^{-1} from the excitation source, with one filter 2 nm to the red and two filters to the blue. For excitation at 473.0 nm, the detection filters are at 505.8, 507.8, 509.8, and 511.8 nm. The 509.8-nm filter is centered on the Raman line. The other filters characterize the background fluorescence level. The PMT detectors have good quantum efficiency at these wavelengths and provide single-photon sensitivity.

Using four detector channels allows us to build a second Raman spectrometer into the same optical system. A second excitation source at 471.3 nm generates a Raman line at the 507.8-nm filter. As before, we have one detection filter centered on the Raman line straddled by three "background" filters to help establish the baseline. With this redundancy, we can implement a measurement methodology that removes sensitivity to drifts in the PMT efficiency and gain, as described in Sec. 4. Special care must be taken to minimize differences in the spatial structure between the two excitation sources, and to control polarization in the excitation and detection optics, as described in the next section.

4 Divided Shifted Raman Spectroscopy

Using LEDs with interference filters gives us the flexibility to choose the excitation wavelength more or less arbitrarily. However, the corresponding Raman lines and the overall signal levels are weaker than that obtained under laser excitation. Using 0.8-nm bandwidth filters and $f/1.3$ optics results in typically 0.5 mW of optical power focused to a 2-mm-diam. spot. Because the spectral widths of the LED excitation sources are much broader than a laser source, the signal-to-background ratio is further reduced. We compensate for these disadvantages by using a high throughput optical system with high sensitivity PMT detectors.

While PMTs have excellent sensitivity, their signal gain can be influenced by temperature variations. In the analog mode, the gain variation can be as much as 20% over a few hours as the PMTs warm up. Because the carotenoid signal is so small compared to the background, this seemingly slow drift translates into roughly one percent of the Raman peak signal per five seconds of measurement time. For measurement times approaching 100 sec, this is a 20% variability in successive measurements.
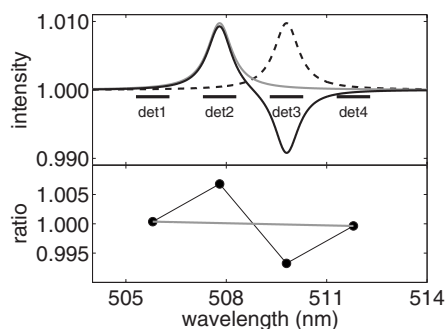
Fig. 2 Top panel: the simulated Raman line with excitation at 473.0 nm (dashed line) and 471.3 nm (gray line) and the ratio of the two (black line). The short horizontal black lines represent the spectral pass bands of the analysis filters. Bottom panel: the values of the ratio of the two Raman signals in the top panel as measured by the four detectors, plotted versus filter wavelength (black circles) and the baseline (gray line). In skin measurements, the background has both slope and curvature (not shown in the figure), although the curvature is always small.

Because of this, standard flat fielding techniques, such as dividing the measurement from a spectrally smooth sample into subsequent measurements, do not work. Variations could be minimized by stabilizing the system's environmental conditions. However, stabilizing PMT response at the 10^{-4} level is challenging, especially for a compact and portable device intended to operate in variable ambient conditions. Instead, we use our two shifted spectral measurements described in Sec. 3 to effectively "flat field" our detectors on a fast time scale while simultaneously extracting the Raman signal. We call our method divided shifted-Raman spectroscopy (DSRS).

For illustrative purposes, two simulated Raman signals are shown in the top panel of Fig. 2. The spectral windows measured by each of the four detection channels are also shown. The dashed line is the Raman signal using 473.0-nm excitation. The Raman peak appears in the third detector and the other three detectors record background levels. The gray line shows the Raman signal using 471.3-nm excitation. In this case, the Raman peak appears in the second detector and the other three detectors record background levels. The black line shows the ratio of the two spectra. The lower panel of Fig. 2 shows the ratio of the optical signal measured by each detector. Note that all effects due to differences in the detector gain and sensitivity and fluorescence collection geometry divide out.

To further illustrate the measurement approach of our LED instrument, we performed similar measurements using two laboratory lasers and a conventional grating spectrometer. In this case, there is far more light available for detection than in the LED instrument. We measured the 1525-cm^{-1} Raman line excited by a doubled Nd:YAG laser at 473 nm and by an argon-ion laser at 476 nm. Typical fluorescence measurements are shown in Fig. 3. The top panel of Fig. 3 shows spectral measurements of light collected from a hand with the two excitation sources. The middle panel shows the 473/476 fluorescence ratio. The short black lines show equally spaced wavelength intervals, similar to what might be transmitted by bandpass filters. The black circles show the average signal over the analysis wavelength ranges. The thin dashed line
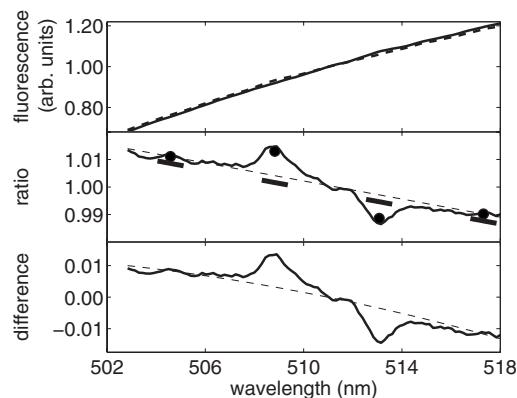

Fig. 3 Top panel: fluorescence measurements on a hand showing the 1525-cm^{-1} Raman line using lasers at 473 nm (dashed line) and 476 nm (solid line). Middle panel: the ratio of the two spectra from the top panel (solid line) and the baseline fit (dashed line). The thick solid lines show the 1-nm bandwidth spectral windows used in the data analysis. The solid circles are plots of the x_i and y_i [see Eq. (2)]. Bottom panel: the difference of the two spectra from the top panel (solid line) and the baseline fit (dashed line) using a similar data analysis approach as in the middle panel. The excitation intensity was 5 mW focused to a 0.5-mm spot diameter. Note that the separation in the laser wavelengths used in this measurement is wider than used in the LED units.

shows a parabolic fit to the background. As is typically the case, the quadratic term is small.

There are similarities in this approach and in the more conventional and successful shifted excitation Raman difference spectroscopy (SERDS) approach.[14] We can imagine that each of the two spectra shown in the top panel of Fig. 3 is represented by a smooth function of wavelength plus some small variation. The fluorescence signal with 473-nm excitation can be written as $\mathcal{S}_{473}(\lambda)=f(\lambda)+g_1(\lambda)$. Similarly, the fluorescence signal with 476-nm excitation can be written as $\mathcal{S}_{476}(\lambda)=f(\lambda)+g_2(\lambda)$. The ratio of these two spectra is

$$\frac{\mathcal{S}_{473}}{\mathcal{S}_{476}} = \frac{f(1+g_1/f)}{f(1+g_2/f)} \approx 1 + \frac{g_1}{f} - \frac{g_2}{f}. \quad (1)$$

If the function f is relatively flat over the two Raman lines represented by the functions g_1 and g_2, division gives the difference of the scaled Raman signals centered about 1. The fact that f is not flat over the two lines and that g_1 and g_2 contain more spectral data than just the Raman lines results in a background that is not perfectly flat. Except for an offset, the ratio (middle panel of Fig. 3) and the difference (bottom panel of Fig. 3) are nearly identical. The important distinction for LED/PMT measurements is that our detectors require rapid flat-fielding for measurements accurate at a level of a few times 10^{-4} of the fluorescence level, which translates into a few percent accuracy in the measurement of the Raman signal strength. In contrast, SERDS would suffer from drift errors on the order of 10^{-2} of the fluorescence level in our application, translating into 100% variation in the Raman signal strength measurements.

We establish the baseline in the DSRS spectrum using the endpoints, which are always "background" measurements. We constrain the baseline by assuming that the ratio measurement

in detector 2 is as far above the baseline as the ratio measurement in detector 3 is below it. These assumptions yield a coupled system of equations for the background and signal strength:

$$y_1 = a + bx_1 + cx_1^2,$$

$$y_2 = a + bx_2 + cx_2^2 + d,$$

$$y_3 = a + bx_3 + cx_3^2 - d,$$

$$y_4 = a + bx_4 + cx_4^2, \quad (2)$$

where the y_i are the ratios of PMT measurements of the two excitation sources, and the x_i are the interference filter passband centers. The parameters a, b, and c are the coefficients of the parabola that best represent the baseline. The parameter d is magnitude of the difference between the Raman signal and the baseline on this relative scale. Note that these equations are derived assuming that d is small (e.g., $d \lesssim 0.01$ as for skin measurements).

When d approaches unity, the DSRS method is inapplicable. This is the regime in which standard Raman measurement techniques can be implemented. However, even high concentration samples with $d \sim 0.3$ can be reliably measured using our technique, because we can include higher order corrections to determine d in Eqs. (1) and (2).

The parameter d is put on an absolute scale by multiplying it by the PMT voltages used in the denominator of y_i. To achieve good reliability, the detector stability needs only to be maintained (or measured) at a few percent level, which is much simpler than the 10^{-4} required without using the DSRS technique. We characterize the PMT response to 1% percent using a calibration LED with known brightness preceding each measurement. Absolute calibration is achieved by measuring the Raman response of a sample with known carotenoid concentration.

With a different set of assumptions, this scheme could be implemented with fewer detectors and we have tested these approaches. We find that instruments with two or three detectors do not give the repeatability or reliability of the four detector design, largely because the fluorescence background has both slope and curvature. The parabolic analysis in Eq. (2) makes it possible to derive a curved baseline with high reliability. A configuration with a greater number of detectors could be used, but the additional redundancy does not seem to offer noticeably better machine performance than what is achieved using four.

In principle, the division analysis method could be used with conventional CCD detection devices. It would be most appropriate when the Raman spectrum was dominated by background fluorescence. The experimental realization of the division technique in this work requires a simple Raman spectrum, such as in resonance measurements. The background measurement points need to be free of any Raman lines. Our implementation of the DSRS technique depends on prior knowledge of detailed spectral features.

When using two independent excitation sources, it is important to make sure that the spatial profile of the two sources is identical. Variations in this profile result from both the structure of the LEDs themselves, but also in the interference filters used to narrow their output spectrum. We do this using a 1-mm-diam, 20-mm-long glass rod. The material was chosen to have a high index of refraction and a low fluorescence level. This rod acts somewhat like a very large diameter optical fiber. The multiple internal reflections remove residual differences in the spatial profile of the two excitation sources. It is also important to make sure the optical polarization of the two sources is identical, and to make sure that the polarization is identical at the beamsplitter preceding each PMT. The Raman signal has the same polarization as the excitation source. This is not true for the background fluorescence. If the collected fluorescence at each PMT is not identical, a markedly different signal-to-background ratio will be measured, and the derived Raman signal strength will be compromised. Special care must be taken because the Fresnel reflection coefficients at 45-deg angles of incidence are typically quite different for the two polarizations in commercial beamsplitters.

5 Benchmark Comparison to Laser-Based Units

A few years ago, Pharmanex® (Provo, Utah) developed a laser-based Raman instrument for detecting carotenoid molecules in human skin tissue. It was based on a larger laboratory research device.[12,21,22] A fiber-coupled laser was focused on the hand, and backward-directed fluorescence was fiber-coupled into a grating spectrometer. The light intensity in the Raman peak was measured in the spectrometer trace. Raman measurements correlate with carotenoid serum levels,[23] and both resonance and nonresonance Raman measurements can be used to identify, quantify, and monitor molecular content in skin tissue.[9,11,24-28]

Pharmanex® developed an arbitrary scale for quantifying carotenoid levels in skin tissue that is proportional to the Raman signal. On this scale, the average American has a reading in the neighborhood of 25,000 for measurements made in the palm of the hand. The palm has the advantage of being relatively homogeneous and melanin-free. Typical scores range from 10,000 to 50,000, similar to the spread of the population seen in Fig. 4, and the measurement uncertainty is less than 3000.

We have performed hundreds of tests comparing the performance of our units and laser-based Raman spectrometers. The results of one test are shown in Fig. 4. For this study, 38 persons repeatedly measured their antioxidant scores on a laser Raman instrument and also on LED Raman instruments over a one-week time period. To within the error of the measurements, the two different kinds of instruments read identically to one another. A straight-line fit to the data in Fig. 4 has a reduced R^2 value of 0.96. The LED Raman instruments also show high repeatability. The vertical error bars in Fig. 4 are the 1σ standard deviations of 20 measurements on two LED Raman units. The average relative standard deviation (RSD) is 9%. This is the 1σ variation in a person's score divided by their mean score and averaged over the 38 persons in this study. The typical RSD is somewhat lower for scores in the 25,000 to 50,000 range.

The LED Raman instruments are accurate in spite of their low intensity illumination of the skin. The optical power on the skin is less than 0.5 mW in a 3.1-mm^2 area. The resulting
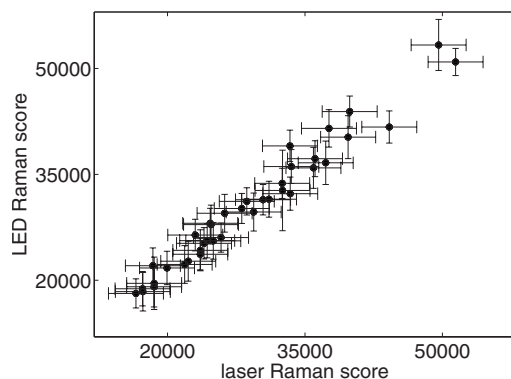
Fig. 4 Comparison of laser-Raman and LED-Raman carotenoid measurements on 38 people. The absolute calibration of the LED instrument was chosen to match the laser-Raman instrument. The vertical error bars are the 1σ standard deviations for 20 measurements on two LED Raman instruments over five days. The horizontal error bars are typical 1σ standard deviation measurements for the laser Raman instruments. The measurement time is two minutes for the LED Raman instrument and three minutes for the laser Raman instruments. To within the measurement uncertainty, this graph shows perfect correlation between the two machines. The reduced R^2 value of a straight line fit is 0.96.

maximum intensity is $0.016 \ \text{W}/\text{cm}^2$, which is $12.5\times$ lower than the maximum permissible exposure for laser radiation of comparable wavelength.[29]

6   Long-Term Calibration Reliability

The LED Raman instruments are designed to have long-term calibration reliability. The optical system includes a photodiode to measure the brightness of the emission sources (PD1 in Fig. 1) and also an additional LED and photodiode to measure the PMT sensitivity (LED3 and PD2 in Fig. 1). These items constitute a set of internal calibration standards for the instrument. They allow us to correct readings for drifts in excitation intensity and PMT sensitivity over time that may arise from temperature variation or component aging.

In normal use, a unit is calibrated at the beginning of a measurement session using a portable Raman standard. All of the PMT, LED, and photodiode values are recorded. Using the internal calibration standards, we correct all readings back to the LED brightness and PMT sensitivities as measured at the time of calibration.

The internal calibration standards are highly robust. Instead of using them to refer to conditions at the beginning of a particular measurement session, they can be used to refer to conditions at a factory calibration. In Fig. 5 we compare the scores measured over a 265-day period determined in two ways. The first is the "normal" way, using calibrations performed at the point of measurement. The second way uses the internal calibration standards to refer back to a single factory calibration. The data in Fig. 5 are a histogram of differences in the scores calculated in these two ways. The overall shift in score is approximately 1%. The 1σ confidence level (68.3%) is ± 1235. A closer evaluation of the data suggests that most of these score differences arise from errors in the calibration at the point of measurement. These data show that the internal
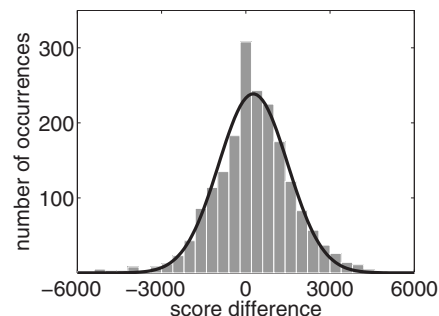

Fig. 5 Histogram of score differences over a 265-day period. The x axis is the difference between the scores determined using on-site calibration (147 different calibration events) and the scores determined using the internal calibration standards. The 1σ width (68.3% confidence level) determined by the Gaussian fit to the data (black line) is ± 1235.

calibration standards are stable over time periods approaching a year, and stability over much longer time periods seems likely.

7   Conclusion

We report on the development of a compact and portable Raman instrument for measuring carotenoid molecules in human skin. Thousands of these have been built and are in routine operation. These units use high sensitivity detectors and a high throughput optical system, making it possible to use incoherent light sources for resonance Raman spectroscopy in a commercial setting. We show repeatability better than 10% on LED Raman instruments and excellent correlation with laser-based Raman spectroscopy measurements. This work represents an important step forward for nonlaboratory *in-vivo* Raman spectroscopy using low intensity excitation. With the expanding availability of ultraviolet LEDs, and considering that many important biomolecules have resonances in the ultraviolet wavelength range, this approach may be useful for other systems.

References

1. A. Rattner and J. Nathans, "Macular degeneration: recent advances and therapeutic opportunities," *Nat. Rev. Neurosci.* **7**, 860–872 (2006).
2. K. Wertz, P. B. Hunziker, N. Seifert, G. Riss, M. Neeb, G. Steiner, W. Hunziker, and R. Goralczyk, "β-carotene interferes with ultraviolet light a-induced gene expression by multiple pathways," *J. Invest. Dermatol.* **124**, 428–434 (2005).
3. H. E. Seifried, S. S. McDonald, D. E. Anderson, P. Greenwald, and J. A. Milner, "The antioxidant conundrum in cancer," *Cancer Res.* **63**, 4295–4298 (2003).
4. J. F. Dorgan, N. A. Boakye, T. R. Fears, R. L. Schleicher, W. Helsel, C. Anderson, J. Robinson, J. D. Guin, S. Lessin, L. D. Ratnasinghe, and J. A. Tangrea, "Serum carotenoids and α-tocopherol and risk of nonmelanoma skin cancer," *Cancer Epidemiol. Biomarkers Prev.* **13**, 1276–1282 (2004).
5. M. Porrini and P. Riso, "Lymphocyte lycopene concentration and DNA protection from oxidative damage is increased in women after a short period of tomato consumption," *J. Nutr.* **130**, 189–192 (2000).
6. J. W. Horton, D. J. White, D. L. Maass, D. P. Hybki, S. Haudek, and B. Giroir, "Antioxidant vitamin therapy alters burn trauma-mediated cardiac NF-kappaB activation and cardiomyocyte cytokine secretion," *J. Trauma* **50**, 397–406 (2001).
7. W. Gellermann, I. V. Ermakov, M. R. Ermakova, and R. W. McClane,

"*In vivo* resonant Raman measurements of macular carotenoid pigments in the young and in the aging human retina," *J. Opt. Soc. Am. A* **19**, 1172–1186 (2002).

8. I. V. Ermakov, M. R. Ermakova, W. Gellermann, and J. Lademann, "Noninvasive selective detection of lycopene and β-carotene in human skin using Raman spectroscopy," *J. Biomed. Opt.* **9**, 332–338 (2004).

9. P. J. Caspers, G. W. Lucasson, E. A. Carter, H. A. Bruining, and G. J. Puppels, "*In vivo* confocal Raman microspectroscopy of the skin: noninvasive determination of molecular concentration profiles," *J. Invest. Dermatol.* **116**, 434–442 (2001).

10. C. J. Frank, D. C. B. Redd, T. S. Gansler, and R. L. McCreery, "Characterization of human breast biopsy specimens with near-IR Raman spectroscopy," *Anal. Chem.* **66**, 319–326 (1994).

11. T. R. Hata, T. A. Scholz, I. V. Ermakov, R. W. McClane, F. Khachik, W. Gellermann, and L. K. Pershing, "Non-invasive Raman spectroscopic detection of carotenoids in human skin," *J. Invest. Dermatol.* **115**, 441–448 (2000).

12. P. S. Bernstein, M. D. Yoshida, N. B. Katz, R. W. McClane, and W. Gellermann, "Raman detection of macular carotenoid pigments in intact human retina," *Invest. Ophthalmol. Visual Sci.* **39**, 2003–2011 (1998).

13. I. V. Ermakov, M. R. Ermakova, and W. Gellermann, "Simple Raman instrument for in vivo detection of macular pigments," *Appl. Spectrosc.* **59**, 861–867 (2005).

14. W. R. Brown and J. J. McGarvey, "The Raman effect and its application to electronic spectroscopies in metal-centered species: Techniques and investigations in ground and excited states," *Coord. Chem. Rev.* **251**, 454–473 (2007).

15. T. Polivka, D. Zigmantas, H. A. Frank, J. A. Bautista, J. L. Herek, Y. Koyama, R. Fujii, and V. Sundstrom, "Near-infrared time-resolved study of the S_1 state dynamics of the carotenoid spheroidene," *J. Phys. Chem. B* **105**, 1072–1080 (2001).

16. T. Polivka and V. Sundstrom, "Ultrafast dynamics of carotenoid excited states -from solution to natural and artificial systems," *Chem. Rev. (Washington, D.C.)* **104**, 2021–2071 (2004).

17. J. Sue and S. Mukamel, "Analysis of fluorescence line shapes and Raman excitation profiles of tetradesmethyl-β-carotene," *J. Chem. Phys.* **88**, 651–665 (1988).

18. M. Yoshizawa, H. Aoki, M. Ue, and H. Hashimoto, "Ultrafast kinetics of excited states in a series of mini- and macro-β-carotenes," *Phys. Rev. B* **67**, 174302 (2003).

19. R. R. Anderson and J. A. Parrish, "The optics of human skin," *J. Invest. Dermatol.* **77**, 13–19 (1981).

20. M. E. Darvin, I. Gersonde, M. Meinke, W. Sterry, and J. Lademann, "Non-invasive *in vivo* determination of the carotenoids *beta*-carotene and lycopene concentrations in the human skin using the Raman spectroscopic method," *J. Phys. D* **38**, 2696–2700 (2005).

21. I. V. Ermakov, M. R. Ermakova, R. W. McClane, and W. Gellermann, "Resonance Raman detection of carotenoid antioxidants in living human tissues," *Opt. Lett.* **26**, 1179–1181 (2001).

22. I. V. Ermakov, R. W. McClane, and W. Gellermann, "Resonant raman detection of macular pigment levels in the living human retina," *Opt. Lett.* **26**, 202–204 (2001).

23. I. V. Ermakov, M. Sharifzadeh, M. Ermakova, and W. Gellermann, "Resonance Raman detection of carotenoid antioxidants in living human tissue," *J. Biomed. Opt.* **10**, 064028 (2005).

24. B. R. Hammond, Jr. and B. R. Wooten, "Validity issues with the in vivo measurements of skin carotenoids using Raman spectroscopy," *J. Invest. Dermatol.* **122**, 544–546 (2004).

25. W. Gellermann, I. V. Ermakov, and P. Bernstein, "Author response," *J. Invest. Dermatol.* **122**, 546–548 (2004).

26. M. Gniadecka, P. A. Philipsen, S. Sigurdsson, S. Wessel, O. F. Nielsen, D. H. Christensen, J. Hercogova, K. Rossen, H. K. Thomsen, R. Gniadecki, L. K. Hansen, and H. C. Wulf, "Melanoma diagnosis by Raman spectroscopy and neural networks: structure alterations in proteins and lipids in intact cancer tissue," *J. Invest. Dermatol.* **122**, 443–449 (2004).

27. A. Nijssen, T. C. Bakker Schut, F. Heule, P. J. Caspers, and D. P. Hayes, "Discriminating basal cell carcinoma from its surrounding tissue by Raman spectroscopy," *J. Invest. Dermatol.* **119**, 64–69 (2002).

28. C. Xiao, D. J. Moore, M. E. Rerek, C. R. Flach, and R. Mendelsohn, "Feasibility of tracking phospholipid permeation into skin using infrared and Raman microscopic imaging," *J. Invest. Dermatol.* **124**, 622–632 (2005).

29. American National Standards for the Safe Use of Lasers, ANSI Z136.1–2000, Table A3.